Laboratory observation of secondary shock formation ahead of a strongly radiative blast wave

J. F. Hansen, M. J. Edwards, and D. H. Froula
Lawrence Livermore National Laboratory, Livermore, California 94550

G. Gregori
LRC-Rutherford Appleton Laboratory, Chilton, Didcot OX11 0QX, United Kingdom

A. D. Edens
Sandia National Laboratory, Albuquerque, New Mexico 87185

T. Ditmire
University of Texas at Austin, Austin, Texas 78712

(Received 17 October 2005; accepted 29 December 2005; published online 8 February 2006)

High Mach number blast waves were created by focusing a laser pulse on a solid pin, surrounded by nitrogen or xenon gas. In xenon, the initial shock is strongly radiative, sending out a supersonic radiative heat wave far ahead of itself. The shock propagates into the heated gas, diminishing in strength as it goes. The radiative heat wave also slows, and when its Mach number drops to two with respect to the downstream plasma, the heat wave drives a second shock ahead of itself to satisfy mass and momentum conservation in the heat wave reference frame; the heat wave becomes subsonic behind the second shock. For some time both shocks are observed simultaneously. Eventually the initial shock diminishes in strength so much that it can longer be observed, but the second shock continues to propagate long after this time. This sequence of events is a new phenomenon that has not previously been discussed in the literature. Numerical simulation clarifies the origin of the second shock, and its position is consistent with an analytical estimate. © *2006 American Institute of Physics*. [DOI: 10.1063/1.2168157]

I. INTRODUCTION

We have conducted experiments comparing the shock expansion in blast waves in which radiative effects are observed to be very different, and we report here our findings, including a new phenomenon that has not previously been observed. The motivation behind this experiment and many other experiments in laboratories around the world[1–9] is an interest in astrophysical shocks that have high Mach numbers and that may be radiative.[10] Astrophysical shocks originating in supernova (SN) explosions[3,11–14] are the most studied, but other astrophysical phenomena (e.g., T Tauri stars[15] and stellar winds[16]) also generate their own shocks. Interstellar space consists of a tenuous plasma capable of propagating shocks over great distances, so shocks are important to understand as they mix up interstellar matter and thus affect mass-loading, stellar formation[17–19] and the history of the Milky Way and other galaxies.

The radiative nature of a shock, coupled with the optical opacity of its surroundings, largely determines the evolution of the shock and its rate of expansion. A SN shock expanding through interstellar space loses energy through radiation, although some energy may be recovered as the shock sweeps up interstellar material. The energy loss rate for the shock can be quantified[20] by the parameter $\varepsilon=-(\mathrm{d}E/\mathrm{d}t)\times(2\pi\rho_0)^{-1}r_s^{-2}(\mathrm{d}r_s/\mathrm{d}t)^{-3}$, where E is the total energy content of the shock, ρ_0 is the density of the ambient interstellar gas, r_s is shock radius, and t is time. In a fully radiative case, in which radiation escapes to infinity, the incoming kinetic energy swept up by a shock is entirely radiated away and the shocked material collapses to a thin shell directly behind the shock. The denominator is then precisely the rate at which kinetic energy is accumulated, and $\varepsilon=1$. For an adiabatic case $\varepsilon=0$ and once the shock has swept up more mass than what was initially present, the shock could be regarded as without characteristic length or time scales, and one would expect the well-known self-similar motion of a Sedov-Taylor blast wave,[21–24] $r_s\propto t^{\alpha}$, where the exponent $\alpha=2/5$. (This assumes that there are no density gradients in the swept region of space.) In a case where radiation removes energy from the shock in an optically thin environment, analytical and numerical studies predict a slower shock expansion, such as $\alpha=2/7$ (the "pressure-driven snowplow"), $\alpha=1/4$ (the "momentum-driven snowplow"; the shock is simply coasting),[10,25] and $2/7<\alpha<2/5$ (the thermal energy of the shocked gas is not completely radiated away).[20,24]

In a case where the environment is not optically thin, which is the case for many experiments including ours, radiation is reabsorbed in the upstream material and if the shock is traveling fast enough a supersonic, radiative heat wave (RHW) breaks away from the shock in a situation analogous to a supercritical shock wave.[23] It has been shown that the shock and RHW will coexist and eventually propagate as $r\propto t^{\alpha}$, where α is larger for the shock.[26] This means that the shock would eventually catch RHW, after which a second state is obtained in which RHW is of the ablative type and the shock moves in a classical Sedov-Taylor trajectory with $\alpha=2/5$. In this paper we report on the additional possibility that prior to the shock catching RHW, the latter

enters a transonic regime, stalls, and generates a second shock. Although our motivation for this experiment was an interest in astrophysical shocks, we should point out that the new phenomenon we describe has not been observed in astrophysical shocks and may not occur there.

II. EXPERIMENT SETUP AND DIAGNOSTICS

We create spherically expanding blast waves in the following fashion: a high-power infrared pulsed laser (1064 nm wavelength) is focused onto the tip of a solid (stainless steel) pin surrounded by an ambient gas (nitrogen or xenon) typically at a pressure of about 1 kPa (density $\rho_0 \sim 10^{-5}$ g/cm^3). The laser pulse is 5 ns in duration with energy ranging from $E_l = 10$ to 200 J (we see no qualitatively different behavior in the blast wave evolution over this energy range). The laser pulse ablates the pin and rapid expansion of ablated material shocks the ambient gas. The initial shock travels radially outward from the pin; most of the shocked gas is concentrated in a shell immediately behind the shock front. We use the term blast wave to refer to shock and shell. The blast wave velocity drops as more and more of the ambient gas is accumulated and set in motion by the passing shock. When the mass of swept up material is much larger than the initially ablated material, the motion of the blast wave becomes self-similar. We can conservatively estimate the radius at which this occurs, assuming that all laser energy is deposited in pin material, heating it uniformly. (The loss of laser energy, e.g., due to misalignment between the laser beam and the pin, and nonuniform heating, will lower our estimated radius.) For example, if the ambient gas is xenon and the laser pulse deposits 10 J in the blast wave, the amount of ablated iron is such that when the blast wave has traveled 0.4 mm it will have swept up a much larger (ten times larger) xenon mass.

To image a blast wave on spatial scales up to ≈5 cm, we use two lenses in a telescope configuration and a gated, single-frame, high-speed CCD camera (2 ns gate), along with a low-energy, green laser pulse ($\lambda = 532$ nm wavelength, 15 ns duration) as a backlighter. The blast wave radius as a function of time is obtained by employing a schlieren technique so that only laser light perturbed by the plasma is imaged; light that has not been deflected is removed at the telescope focal point by a small (≈500 μm) beam block. With this method, image brightness corresponds to the spatial derivative of plasma electron density, and the blast wave structure is readily seen. Additionally, glow from a heated plasma can be seen in the images since no monochromatic filter was placed in front of the camera. Schlieren images were obtained from 5 ns up to 35 μs after the initial, ablative laser pulse.

III. RESULTS

Examples of images using nitrogen as the ambient gas can be seen in Fig. 1. In each image, the laser ablating the target pin is incident from the left. The pin is clearly visible, as is the expanding blast wave. [Note that the shock is not exactly centered on the pin and also is not perfectly spherical; deviation from sphericity is evident on the laser side of the pin. A two-dimensional (2D) computer simulation (computed by the CALE code,[27] an arbitrary Lagrangian-Eulerian code including both hydrodynamic and radiative effects) shows how laser-plasma interaction causes preionization and preheating of the plasma on the laser side. The shock then propagates through a nonuniform plasma, leading to a nonuniform shock expansion. This effect is further discussed by Edens *et al.*[28]] The shock expansion settles (to within measurement error) into the Sedov-Taylor relationship for a blast wave $r_s \propto t^{2/5}$ after an initial, brief, non-self-similar phase. This is expected for a shock in which the net radiative effects are small. [It also appeared that $r_s \propto (E_l/\rho_0)^{1/5}$, where E_l is the laser energy, also consistent with a Sedov-Taylor blast wave.]

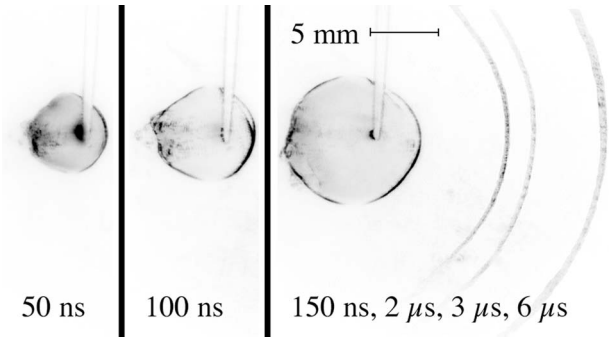

FIG. 1. Blast wave expansion through ambient nitrogen gas (1.3 kPa) at times $t = 150$ ns to 6 μs after an ablative laser pulse (energy $E_l = 10$ J, duration 5 ns) is focused on a solid pin (visible in images, pointed down). The laser pulse was incident from the left. The shock is spherical (except on the laser side due to laser-plasma interaction) and its growth is consistent with a Sedov-Taylor blast wave. The image to the right ($t = 150$ ns to 6 μs) is a composite of four images (with overlapping pin locations).

Examples of images using xenon as the ambient gas can be seen in Fig. 2. With its higher atomic number, xenon radiates more strongly than nitrogen, and there are notable differences in the images pointing to more influential radiative effects: (a) plasma emission from preheated gas, that is, gas heated by the radiation from the shock, is clearly visible as a glow surrounding the shock at early times ($t \lesssim 400$ ns). (b) The shock expansion is slower than in nitrogen, even when accounting for the $r_s \propto \rho^{-1/5}$ factor from the higher density of xenon. We also observe that the shock weakens ($t \approx 1$ μs to 4 μs) and gets increasingly difficult to detect. Before the initial shock becomes undetectable ($t \approx 8$ μs), a second shock forms out ahead of the initial shock. This second shock is a phenomenon that has not previously been discussed in the literature in this context. It is not surrounded by a glow of preheated gas, and it continues to propagate long after the initial shock can no longer be detected. Examples of shocks in xenon at higher laser energies are shown in Fig. 3. The same qualitative evolution occurs at these higher laser energies. A plot of shock radius versus time, shown in Fig. 4, clearly shows a "step" where the second shock forms. This step must be made by a second shock forming; the initial shock cannot suddenly jump ahead.

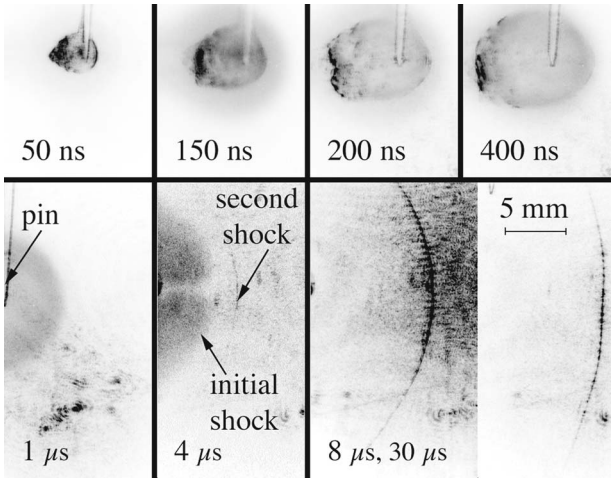

FIG. 2. Blast wave expansion through ambient Xe gas (1.3 kPa) at times $t=50$ ns to 30 μs after an ablative laser pulse (energy $E_l=10$ J, duration 5 ns) is focused on a solid pin (visible in images, the pin location in the bottom row of images is at the left edge of each image). The laser pulse was incident from the left. The initial shock is strongly radiative (supercritical) and preheats the ambient gas. At $t=150$ ns both the initial shock and the preheated gas ahead of it are clearly visible. At $t\approx 1$ μs the initial shock begins to dissipate, and the shock front is no longer obviously sharp. At $t\approx 4$ μs a second shock appears (located at the tip of the arrow), ahead of the initial shock. The second shock continues to expand while the initial shock gradually becomes undetectable. The final image ($t=8$ μs, 30 μs) is a composite of two images (with overlapping pin locations).

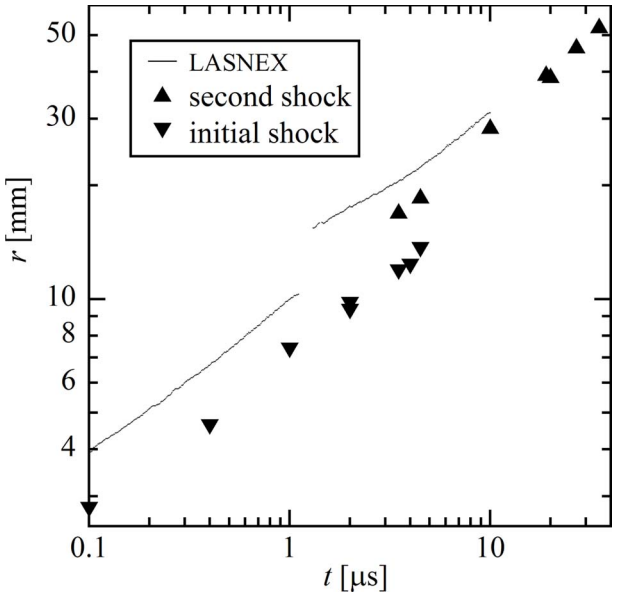

FIG. 4. Measured shock radius vs time in experimental images of shocks in xenon. Ablative laser energy $E_l\approx 100-200$ J; duration 5 ns. Note the step in radius around the transition time (~ 4 μs) when both shocks are visible. The curve is from a LASNEX simulation and shows the largest radius at which the compression $\eta\geqslant 1.25$. This curve shows the same step in radius, although at an earlier time (we can "detect" the second shock earlier in a numerical simulation than in the experiment). The slope of the curve for the second shock increases as the shock sharpens up. The energy for this calculation was $E=30$ J, less than the actual laser energy but still likely an overestimate of how much energy is deposited in the blast wave [most of the laser energy is lost, e.g., in the laser-focusing channel (Ref. 28) and through reflection].

IV. COMPARISON TO NUMERICAL SIMULATION

To help interpret our experimental results we ran a 1D numerical simulation using the LASNEX code;[29,30] see Fig. 5. Radiation was treated in the multigroup diffusion approximation, which is valid when the radiation field is nearly isotropic. In this experiment this means having a large enough optical depth in the RHW, a condition that is satisfied reasonably early in the experiment (see later). We also saw that more sophisticated radiation treatments gave very similar answers for the entire evolution. Opacities were calculated in line using a screened hydrogenic (SH) approximation that reproduces the average degree of ionization reported for very similar conditions using a more sophisticated model[31] to within $\sim 25\%$. The early time laser interaction region was treated with a time-dependent nonlocal thermodynamic equilibrium (non-LTE) version of the SH model. At later times it made little difference to the overall energetics and evolution of the blast wave if LTE was assumed or not. The equation of state (EOS) was computed using either QEOS[32] in LTE, or from the non-LTE population distribution in non-LTE. More sophisticated models may alter the details of the predictions, but based on a number of calculations in which we have varied the EOS and opacities, we do not expect the qualitative picture to change. In any event, the simulation captures the observed blast wave behavior rather well.

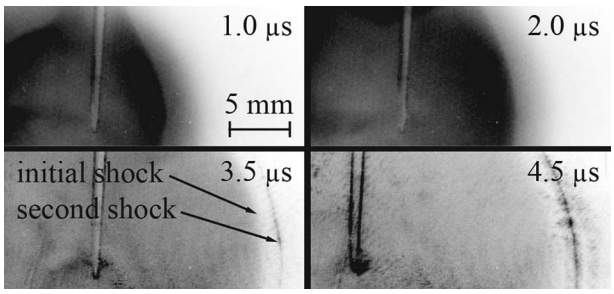

FIG. 3. Blast wave expansion through ambient Xe gas (1.3 kPa) at times $t=1.0$ μs to 4.5 μs. Ablative laser pulse energy $E_l\approx 120$ J; duration 5 ns. At $t=3.5$ μs both initial and second shocks are clearly visible.

Qualitatively the simulation follows the discussion of this process given by Reinicke and Meyer-ter-vehn,[26] but also includes the birth of the second shock wave. Before presenting a more detailed description of the computational results, we summarize them here. At early times, the initial shock (which we will refer to as S1) is fast enough to radiate very strongly. The radiation mean free path in the cold ambient gas ahead of S1 is relatively short, resulting in the formation of a supersonic RHW, which propagates in advance of S1. (Note that if the surrounding gas is optically thin, the energy is instead lost, transported to "infinity," and RHW would not form.) As S1 continually slows down, it radiates less and less. The radiated power soon drops below the rate at which S1 sweeps up energy from gas heated by the RHW, and eventually S1 slows below the minimum velocity at which a shock could have created a supersonic radiative heat wave in the first place. At this time RHW is still far ahead of S1, but its velocity has also been diminishing rapidly because of expansion and a rapidly weakening driving source. Before S1 is able to catch it, RHW becomes transonic, and eventually gives birth to a second shock wave

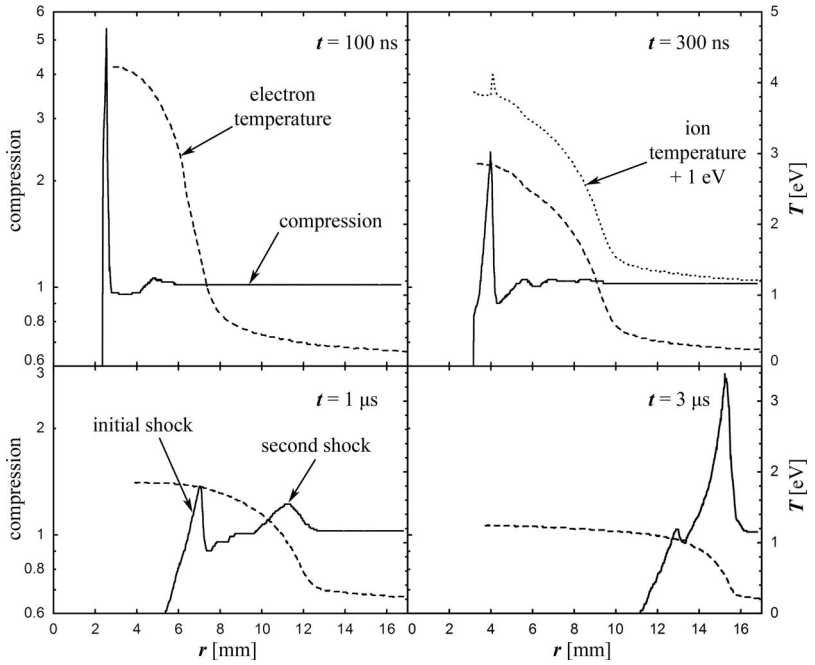

FIG. 5. Compression and electron temperature vs radius in the Xe plasma at four different stages of the blast wave evolution. Note the initial shock dissipating and the second shock being born at the radiative heat wave front. Also illustrated in the plot (at $t=0.3$ μs) is the ion temperature, which is in equilibrium with the electron temperature, except in the thin relaxation layer behind the shock front. This layer is not fully resolved in the simulation shown, and the temperature excursions are not as high as they would be in reality. This is partly responsible for the apparent continuous nature of the electron temperature at the shock. In reality the electrons are essentially adiabatic at the shock, and do undergo a smaller "jump" in temperature (Ref. 23) In a simulation of the first few hundred nanoseconds with ten times the spatial resolution, we resolve the relaxation layer much better, yet the other details (and conclusions from those) remain unchanged.

(which we will refer to as S2). RHW then falls behind S2, which itself is too slow to be radiative. By the time S2 is formed S1 is relatively weak (Mach number $M\approx 2$), and it continues to weaken as it propagates in the downstream material of S2. After S2 has roughly doubled its radius, it is no longer influenced by the details of how it was formed, and the shock trajectory closely assumes that of a self-similar Sedov-Taylor blast wave. We will now elaborate on this sequence of events, beginning with the motion of S1.

At the end of the laser pulse ($t=5$ ns), motion is still strongly influenced by the details of the initial conditions. S1 is traveling in excess of 60 km/s and is strongly radiative. This is consistent with the results of Bouquet *et al.*,[9] who find that shocks at this speed (and at higher densities) are strongly radiative. To help quantify the importance of radiation we have calculated the (inverse) Boltzmann number $\mathrm{Bo}^{-1}=\sigma T^4/v_s\rho_0 c_v T$ for this time from the numerical simulation. The denominator in this equation is the flux required to heat the upstream material (flow speed $v_s=\mathrm{d}r_s/\mathrm{d}t$, density ρ_0) to the temperature T of the downstream plasma, while the numerator would be approximately the flux delivered from the hot, downstream plasma to the upstream material. When these two fluxes are equal, the shock is said to be critical, and the upstream material is heated by radiation to the temperature of the downstream plasma, the "critical" temperature $T=T_c$. When the radiative flux exceeds this value, the shock is said to be supercritical. In this case, the upstream plasma is still heated to the temperature $T>T_c$ of the downstream plasma, and the "excess" flux is used to increase the extent of the radiative precursor. The flux F_R actually emitted through the shock by the downstream plasma in this case is calculated to be somewhat less than σT^4 because the plasma is too small to be optically thick. Nevertheless, the calculated value of F_R still exceeds the calculated value of the denominator $v_s\rho_0 c_v T$ by ~ 50, and the shock is supercritical at this time. We note that the temperature directly behind the shock spikes above the downstream temperature T we refer to previously, but rapidly relaxes toward T. An excellent discussion of the radiating shock structure, including many details omitted here, can be found in Zel'dovich and Raizer,[23] in which the radiation field is formulated in the diffusion approximation to make the problem tractable. Other discussions presenting additional insights and extensions can be found in the excellent texts of Mihalas and Mihalas[33] and Castor.[34]

The strongly radiative S1 drives a highly supersonic RHW far out ahead of itself (RHW radius $r_h\approx 2.5$ mm); this heat wave is driven by radiation, not thermal electrons, as the radiative conductivity is at least two orders of magnitude greater than the electron thermal conductivity [e.g., at $T\sim 2.5$eV we calculate ~ 5400 W/(m$\times$K) for the radiation and 7.3 W/(m$\times$K) for the electrons] and additionally we see no noticeable difference in the numerical simulation if electron heat conduction is explicitly omitted. The S1 compression η is very high ($\eta>20$), a feature consistent with strongly radiating shocks. By $t\approx 20$ ns, the memory of the details of the initial conditions is no longer apparent. S1 has expanded to $r_s\approx 1.4$ mm and slowed to ~ 30 km/s, but is still strongly radiative ($\varepsilon\approx 0.8$). However, only about one-eighth of the total energy now resides inside S1 with the remainder in RHW, which extends to $r_h\approx 4$ mm. (As a result, the subsequent evolution of RHW cannot be much affected by S1.)

As S1 continues to slow down, its ability to radiate diminishes rapidly. Eventually S1 sweeps up energy from the material heated by RHW faster than it radiates and thereafter the energy inside S1 gradually increases ($\varepsilon<0$). This should result in a slight acceleration of the blast wave, but the experimental measurement is not accurate enough to verify this. By $t=300$ ns, S1 has expanded to $r_s\approx 4$ mm and its velocity has fallen to ~ 6 km/s, or twice the speed of sound

in the RHW plasma into which S1 propagates. The S1 compression is $\eta \approx 3$, consistent with a relatively weak shock wave (this is just like the point explosion with counterpressure discussed by Zel'dovich and Raizer[23]). We calculate that a shock born at 6 km/s in cold xenon gas would be too slow to be strongly radiative. Also, a shock at this speed but free of the significant pressure of the preheated RHW plasma would have a compression $\eta \approx 7$ (where the additional compression above the $\gamma = 5/3$ strong shock limit of $\eta = 4$ is simply caused by ionization losses in the xenon).

We turn now to details of the RHW. At early time the plasma inside the RHW is optically thin and the radiation wave is essentially a bleaching wave. However, as RHW expands and cools, the optical depth inside the wave rapidly increases, reaching 10 by $t \approx 200$ ns. By $t \approx 300$ ns its radius is about twice the shock radius ($r_h \approx 9$ mm) and its velocity has dropped to that of S1. From here on S1 gradually makes ground on the stalling RHW, but before S1 can catch RHW the latter enters the transonic regime (relative to the sound speed in the hot plasma behind RHW) and begins to drive a nonlinear disturbance that eventually ($t \approx 1.2$ μs) breaks into a shock (which we will refer to as S2). At this time RHW drops behind S2.

Because the formation of S2 is a new result we have gone to some effort to ensure that our interpretation is correct. Most importantly, we collected a large amount of experimental data around the transition time (including shocks in xenon-nitrogen mixes that we will expand upon at a later date), e.g., Fig. 4. It categorically shows S1 and S2 simultaneously and follows their evolution. We also performed two confirmatory LASNEX calculations. In the first we took the RHW temperature distribution well before the formation of S2 and imposed it in a stationary, uniform xenon gas. As expected, RHW advanced and S2 formed just as in the full calculation. In the second calculation, we used a spherical piston to drive a shock with the same trajectory as in the full calculation (where the shock was driven by the laser). This second calculation produced nearly identical results to the full calculation, demonstrating that the observed dynamics result from the radiative nature of S1, and are not substantially influenced by radiation from the target. Any heating of the gas as a result of target radiation would be prompt, and we see no evidence of this. The results of the second calculation were confirmed experimentally by a limited set of shots on graphite pins, which yielded the same results. Also, what makes our interpretation unambiguous is that the radiation from a blast wave in xenon drives secondary blast waves off objects placed some distance away, before the original blast wave reaches the objects. (The objects are also well out of the way of the laser beam.) This does not occur when we use nitrogen gas. We have seen this in several experiments at two different laser facilities.

V. COMPARISON TO ANALYTICAL ESTIMATE

Finally, we compared the observed formation location of S2 to the following simple, analytical estimate for where S2 forms.

Consider the simple 1D fluid equations for the conservation of mass, $\rho_1 u_1 = \rho_2 u_2$ and momentum $p_1 + \rho_1 u_1^2 = p_2 + \rho_2 u_2^2$ in the lab frame of RHW, where subscript 1 denotes the region ahead of RHW, and subscript 2 denotes the region behind RHW. Assuming an ideal gas (so that $p = \rho c^2$, where c is the speed of sound) we combine these to obtain

$$\frac{\rho_2}{\rho_1} = \frac{c_1^2 + u_1^2 \pm \sqrt{(c_1^2 + u_1^2)^2 - 4c_2^2 u_1^2}}{2c_2^2}. \quad (1)$$

A supersonic ($u_1 > c_1$) RHW and a real compression $\eta \equiv \rho_2/\rho_1$ requires $u_1 \geqslant c_2 + \sqrt{c_2^2 - c_1^2} \approx 2c_2$ (where the approximation is valid because the temperature behind RHW is much higher than the temperature before it), i.e., it requires the mixed Mach number $M \equiv u_1/c_2 \geqslant 2$. Once the Mach number drops to 2, RHW can no longer fulfill Eq. (1), and a shock (S2) forms at RHW. This is a standard result in heat front physics and is analogous to when a blast wave forms ahead of a fireball.[23,33,35] S2 immediately moves ahead of RHW and acts to slow down u_1 so that RHW is now subsonic (satisfying $u_1 \leqslant c_2 - \sqrt{c_2^2 - c_1^2} \approx c_1^2/2c_2$). To estimate when RHW slows to Mach 2 and what its radius r_h then is, we can assume a radiative conductivity of the ambient gas of the form $\chi = \chi_0 \rho^a T^b$ and use Barenblatt's solution for an instantaneous point release of energy.[26,36] (A point source is a reasonable estimate[26] because most of the energy that S1 can lose through radiation is lost at an early stage when there is a large separation between S1 and RHW.) Using values for our experiment in xenon (with the deposited energy E calculated from Sedov-Taylor's equation for a blast wave using $\rho_0 = 78$ g/m^3 and $\gamma = 1.2$) and $\chi = 10^{-44} \rho^{-2.2} T^{10}$ in SI units, we find that the RHW Mach number drops to Mach 2 when $r_h \approx 10$ mm. In the experiment we first observed S2 with $r_h \approx 12$ mm, in reasonable agreement with the analytical estimate, particularly considering that the heat front is not sharp, and it takes some time before S2 forms and becomes observable.

VI. SUMMARY

From all the above, we summarize the blast wave evolution in xenon in the following steps: (1) The laser energy is deposited in pin material that then becomes very hot. (2) The heated pin material expands rapidly, pushing at the surrounding gas, setting up a strong, radiative S1. (3) Radiation from S1 heats the surrounding gas. The flux is high enough that S1 is supercritical, driving a supersonic RHW that travels rapidly outward, leaving a large separation between S1 and RHW. (4) S1 sweeps up enough material that the details of its initial conditions become unimportant. (5) S1 slows and its ability to radiate efficiently quickly decreases. (6) S1 is traveling into the counterpressure of hot RHW plasma, which is becoming comparable to the ram pressure; the Mach number drops rapidly, and the post-shock compression reduces correspondingly. (7) When the Mach number for RHW reaches ~2, RHW stalls and creates S2. (8) S1 continues to weaken until it dissipates. (9) S2 is essentially nonradiative and once it has swept up enough mass (doubled its initial radius), it propagates like $r_s \propto t^{2/5}$, provided it remains strong.

ACKNOWLEDGMENTS

We thank Dwight Price and the staff at the Janus facility (where the experiments were conducted) for their valuable assistance.

This work was performed under the auspices of the U. S. Department of Energy by the University of California, Lawrence Livermore National Laboratory under Contract No. W-7405-Eng-48.

[1] J. C. Bozier, G. Thiell, J. P. LeBreton, S. Azra, M. Decroisette, and D. Schirmann, Phys. Rev. Lett. **57**, 1304 (1986).
[2] J. Grun, J. Stamper, C. Manka, J. Resnick, R. Burris, J. Crawford, and B. H. Ripin, Phys. Rev. Lett. **66**, 2738 (1991).
[3] B. A. Remington, D. Arnett, R. P. Drake, and H. Takabe, Science **284**, 1488 (1999).
[4] D. Ryutov, R. P. Drake, J. Kane, E. Liang, B. A. Remington, and W. M. Wood-Vasey, Astrophys. J. **518**, 821 (1999).
[5] K. Shigemori, T. Ditmire, B. A. Remington, V. Yanovksy, D. Ryutov, K. G. Estabrook, M. J. Edwards, A. J. MacKinnon, A. M. Rubenchik, K. A. Keilty, and E. Liang, Astrophys. J. **533**, 159 (2000).
[6] H. F. Robey, J. O. Kane, B. A. Remington, R. P. Drake, O. A. Hurricane, H. Louis, R. J. Wallace, J. Knauer, P. Keiter, D. Arnett, and D. D. Ryutov, Phys. Plasmas **8**, 2446 (2001).
[7] P. A. Keiter, R. P. Drake, T. S. Perry, H. F. Robey, B. A. Remington, C. A. Iglesias, R. J. Wallace, and J. Knauer, Phys. Rev. Lett. **89**, 165 003 (2002).
[8] X. Fleury, S. Bouquet, C. Stehle, M. Koenig, D. Batani, A. Benuzzi-Mounaix, J.-P. Chieze, N. Grandjouan, J. Grenier, T. Hall, E. Henry, J.-P. Lafon, S. Leygnac, V. Malka, B. Marchet, H. Merdji, C. Michaut, and F. Thais, Laser Part. Beams **20**, 263 (2002).
[9] S. Bouquet, C. Stehle, M. Koenig, J.-P. Chieze, A. Benuzzi-Mounaix, D. Batani, S. Leygnac, X. Fleury, H. Merdji, C. Michaut, F. Thais, N. Grandjouan, T. Hall, E. Henry, V. Malka, and J.-P. J. Lafon, Phys. Rev. Lett. **92**, 225 001 (2004).
[10] J. M. Blondin, E. B. Wright, K. J. Borkowski, and S. P. Reynolds, Astrophys. J. **500**, 342 (1998).
[11] E. Müller, B. Fryxell, and D. Arnett, Astron. Astrophys. **251**, 505 (1991).
[12] J. I. Reed, J. J. Hester, A. C. Fabian, and P. F. Winkler, Astrophys. J. **440**, 706 1995).
[13] G. Sonneborn, C. S. J. Pun, R. A. Kimble, T. R. Gull, P. Lundqvist, R. McCray, P. Plait, A. Boggess, C. W. Bowers, A. C. Danks, J. Grady, S. R. Heap, S. Kraemer, D. Lindler, J. Loiacono, S. P. Maran, H. W. Moos, and B. E. Woodgate, Astrophys. J. Lett. **492**, L139 (1998).
[14] N. Bartel, M. F. Bietenholz, M. P. Rupen, A. J. Beasley, D. A. Graham, V. I. Altunin, T. Venturi, G. Umana, W. H. Cannon, and J. E. Conway, Science **287**, 112 (2000).
[15] B. Reipurth and G. Sandell, Astron. Astrophys. **150**, 307 (1985).
[16] J. R. Jokipii, C. P. Scott, and M. S. Giampapa, in *Cosmic Winds and the Heliosphere* (University of Arizona Press, City, 1997).
[17] C. F. McKee and B. T. Draine, Science **252**, 397 (1991).
[18] D. A. Allen and M. G. Burton, Nature **363**, 54 (1993).
[19] R. I. Klein and D. T. Woods, Astrophys. J. **497**, 777 (1998).
[20] E. Cohen, T. Piran, and R. Sari, Astrophys. J. **509**, 717 (1998).
[21] G. I. Taylor, Proc. R. Soc. London, Ser. A **201**, 159 (1950).
[22] L. I. Sedov, *Similarity and Dimensional Methods in Mechanics* (Academic, New York, 1959).
[23] Y. B. Zeldovich and Y. P. Raizer, *Physics of Shock Waves and High-Temperature Hydrodynamic Phenomena* (Academic, New York, 1966).
[24] E. Liang and K. Keilty, Astrophys. J. **533**, 890 (2000).
[25] C. F. McKee and J. P. Ostriker, Astrophys. J. **218**, 148 (1977).
[26] P. Reinicke and J. Meyer-ter-Vehn, Phys. Fluids A **3**, 1807 (1991).
[27] R. T. Barton, in *Numerical Astrophysics*, edited by J. M. Centrella, J. M. LeBlanc, and R. L. Bowers (Jones and Bartlett, Boston, 1985), Vol. 482.
[28] A. D. Edens, T. Ditmire, J. F. Hansen, M. J. Edwards, R. G. Adams, P. Rambo, L. Ruggles, I. C. Smith, and J. L. Porter, Phys. Plasmas **11**, 4968 (2004).
[29] G. B. Zimmerman and W. L. Kruer, Comments Plasma Phys. Controlled Fusion **2**, 51 (1975).
[30] G. B. Zimmerman and R. M. More, J. Quant. Spectrosc. Radiat. Transf. **23**, 517 (1980).
[31] J. M. Laming and J. Grun, Phys. Rev. Lett. **89**, 125 002 (2002).
[32] R. M. More, K. H. Warren, D. A. Young, and G. B. Zimmerman, Phys. Fluids **31**, 3059 (1988).
[33] D. Mihalas and B. Weibel Mihalas, *Foundations of Radiation Hydrodynamics* (Oxford University Press, Oxford, 1984).
[34] J. I. Castor, *Radiation Hydrodynamics* (Cambridge University Press, Cambridge, 2004).
[35] S. P. Hatchett, *UCRL-JC-108 348 Ablation Gas Dynamics of Low-Z Materials Illuminated by Soft X-Rays* (Lawrence Livermore National Laboratory, City, 1991). Copies may be obtained from the National Technical Information Service, Springfield, VA 22161.
[36] G. I. Barenblatt, *Similarity, Self-Similarity and Intermediate Asymptotics* (Consultants Bureau, New York, 1979).